Published in final edited form as:

Nature. ; 481(7382): 530–533. doi:10.1038/nature10735.

Structure of the C-terminal Region of a KCNH Channel

Tinatin I. Brelidze[1], **Anne E. Carlson**[1], **Banumathi Sankaran**[2], and **William N. Zagotta**[1]

[1]Department of Physiology and Biophysics, University of Washington School of Medicine, Box 357290, Seattle, WA 98195-7290

[2]Berkeley Center for Structural Biology, Lawrence Berkeley National Laboratory, 1 Cyclotron Road, BLDG 6R2100, Berkeley, CA 94720, USA

Abstract

The KCNH family of ion channels, comprising *ether-à-go-go* (EAG), EAG-related gene (ERG), and EAG-like (ELK) K^+ channel subfamilies, is crucial for repolarization of the cardiac action potential[1], regulation of neuronal excitability[2], and proliferation of tumor cells[3]. The C-terminal region of KCNH channels contains a cyclic nucleotide-binding homology domain (CNBHD) and C-linker that couples the CNBHD to the pore[4]. The C-linker/CNBHD is essential for proper function and trafficking of ion channels in the KCNH family[5–9]. However, despite the importance of the C-linker/CNBHD for the function of KCNH channels, the structural basis of ion channel regulation by the C-linker/CNBHD is unknown. Here we report the crystal structure of the C-linker/CNBHD of *zebrafish* ELK channels at 2.2 Å resolution. While the overall structure of the C-linker/CNBHD of zELK channels is similar to the cyclic nucleotide-binding domain (CNBD) structure of the related HCN channels[10], there are dramatic differences. Unlike the CNBD of HCN, the CNBHD of zELK displays a negatively charged electrostatic profile that explains the lack of binding and regulation of KCNH channels by cyclic nucleotides[4,11]. Instead of cyclic nucleotide, the binding pocket is occupied by a short β-strand. Mutations of the β-strand shift the voltage dependence of activation to more depolarized voltages, implicating the β-strand as an intrinsic ligand for the CNBHD of zELK channels. In both zELK and HCN channels the C-linker is the site of virtually all of the intersubunit interactions in the C-terminal region. However, in the zELK structure there is a reorientation in the C-linker so the subunits form dimers instead of tetramers as observed in HCN channels. These results provide a structural framework for understanding the regulation of ion channels in the KCNH family by the C-linker/CNBHD and may guide the design of specific drugs.

Address for correspondence: William N. Zagotta, Ph.D., Department of Physiology and Biophysics, University of Washington School of Medicine, Box 357290, Seattle, WA 98195-7290, Tel.: 206-685 -3878; Fax: 206-543-0934; zagotta@u.washington.edu.

AUTHOR CONTRIBUTIONS

T.I.B. and W.N.Z. conceived the experiments. T.I.B. performed the crystallographic experiments, and B.S. helped with the crystallographic data analysis. A.E.C. and W.N.Z. performed the electrophysiology experiments and data analysis. T.I.B. and W.N.Z. wrote the manuscript.

AUTHOR INFORMATION

Atomic coordinates and structure factors for the reported crystal structures have been deposited with the Protein Data Bank under accession codes 3UK5, 3UKN, 3UKT, 3UKV (See Supplementary Table 1 for identifications). Reprints and permissions information is available at www.nature.com/reprints. The authors declare no competing financial interests. Correspondence and requests for materials should be addressed to W.N.Z (zagotta@u.washington.edu).

KCNH channels are voltage-gated K^+ channels that regulate the electrical excitability of heart and nerve cells. Similar to other K^+ selective channels, KCNH channels are composed of four subunits surrounding a centrally located pore. Each subunit contains a voltage-sensor domain (transmembrane segments S1–S4), and a pore domain (transmembrane segments S5–S6 and an intervening pore-forming loop)[4] (Fig. 1a). KCNH channels have a Per-Arnt-Sim (PAS) domain in the N-terminal region and a C-linker and CNBHD in the C-terminal region[4,12] (Fig. 1a). Many of the unique gating properties of KCNH channels arise from these intracellular domains[5–7,13,14]. While the structure of the N-terminal region has been solved for ERG channels[12,15–17], there is no structural information on the C-linker/CNBHD on any of the KCNH channels.

KCNH channels are part of a large family of cyclic nucleotide-regulated channels that includes the hyperpolarization-activated cyclic nucleotide-modulated (HCN) and cyclic nucleotide-gated (CNG) channels (Supplementary Fig. 1a). Unlike HCN and CNG channels[18], KCNH channels are not regulated by direct binding of cyclic nucleotides[4,11]. Instead, it has been suggested that the CNBHD of KCNH channels may be an orphan receptor for a yet unidentified channel regulator[19]. Indeed, it has been recently shown that mEAG channels are regulated by the direct binding of flavonoids to the C-linker/CNBHD[19]. In addition, the C-linker/CNBHD has been shown to interact with the N-terminal PAS domain and regulate gating[6–8]. Mutations in both of these regions in hERG channels cause a Long-QT Syndrome (LQTS), a heart arrhythmia that can cause cardiac death[20]. Therefore the C-linker/CNBHD is an important regulatory domain in KCNH channels.

To understand the role of the C-linker/CNBHD in KCNH channel function we sought to determine the X-ray structure of the C-linker/CNBHD of an ion channel in the KCNH family. Using a screen based on fluorescence-detection size-exclusion chromatography (FSEC)[21], we identified the C-linker/CNBHD of *Danio rerio* (zebrafish) ELK as a potential candidate for crystallization. zELK shares substantial sequence similarity with mammalian ELK channels (Supplementary Fig. 1c).

Expression of zELK channels in *Xenopus laevis* oocytes gave rise to robust voltage-activated K^+ currents with electrophysiological characteristics similar to the ones reported previously for vertebrate ELK channels[22–25] (Fig. 1b). zELK channels were activated by depolarizing voltage steps and showed inactivation at voltages >+40 mV (Fig. 1b). The half-maximal activation voltage ($V_{1/2}$) was −45.3±3.2 mV (n=18) with a slope of e-fold per 13.8±0.6 mV (n=18) (Supplementary Fig. 1b). In comparison, hELK2 channels activate with $V_{1/2}$ of −22.8±0.5 mV and a slope of 18.1±0.4 mV, and inactivate at voltages >+20 mV[22]. As previously observed for mEAG and hERG channels[4,11], application of cAMP had no effect on the currents through zELK channels (Supplementary Fig. 1b).

The C-linker/CNBHD of zELK channels crystallized in two space groups, $C222_1$ and $P12_11$, and diffracted X-rays to 2.2 and 2.3 Å resolution respectively (Supplementary Table 1). The structure of the zELK C-linker/CNBHD was solved by the single-wavelength anomalous dispersion (SAD) phasing method using selenomethionine derivative crystals.

The crystal structure revealed that the C-linker of zELK channels consists of six α-helices (αA'-αF') with αA' and αB' helices forming an antiparallel helix-turn-helix motif. The CNBHD consists of eight β-strands forming an antiparallel β-roll, three α-helices (αA-αC), and a short β-strand (β9) following the αC-helix (Fig. 2a). The general architecture of the CNBHD of zELK is similar to the fold of CNBDs in other proteins[26].

While the overall folds of the CNBHDs of zELK and HCN2 channels are similar, superposition of the two structures reveals remarkable differences (Fig. 2b and Supplementary Fig. 2a). The RMSD for α carbons of the two structures (residues 626–740 of zELK and residues 523–635 of HCN2[10]) is 4.7 Å with the largest differences observed for the three α helices in the CNBHD. The αA and αB-helices of zELK are moved away from the cavity formed by the β-roll that serves as the cyclic nucleotide-binding pocket in other CNBD containing proteins. The αA-helix is moved by about 4.5 Å and the αB-helix is moved by about 3.4 Å relative to their positions in the cAMP-bound form of HCN2. The position of αA of zELK is similar to the position of αA in cAMP-bound MlotiK channels[27] and the positions of αB is similar to the unliganded MlotiK channels[27–29] (Supplementary Fig. 3). The differences in the αC-helix are even more dramatic. The αC-helix of zELK is shorter and bent, and is followed by a short β-strand, β9 (Fig. 2b). These differences all reside in the α-helices of the CNBD that undergo ligand-dependent conformational changes in HCN and CNG channels.

Out of the ten residues that directly interact with cAMP in HCN2 channels only three (V667, L677 and G684) are conserved in zELK channels (Supplementary Fig. 4). Moreover, most of the residues in the phosphate-binding cassette of HCN2, including R591, are not conserved, and the αP-helix is missing in zELK. The electrostatic profiles of the CNBHD of zELK and HCN2 channels reveal that the putative ligand binding pocket formed by the β-roll cavity is negatively charged for zELK but positively charged for HCN2 channels (Fig. 2c and d). The negatively charged electrostatic profile would not be favorable for binding of a negatively charged cyclic nucleotide. Consistent with this, crystallization of zELK in the presence of 5 mM cAMP did not reveal any new electron density corresponding to cAMP (Supplementary Table 1, data not shown). These differences in the CNBD structures likely account, at least in part, for the lack of cyclic nucleotide regulation of KCNH channels[4,11].

The zELK CNBHD structure displays another unique feature: the β9-strand following the αC-helix forms direct interactions with the β-roll cavity in zELK channels (Fig. 2e and Supplementary Figs. 2b and 5). Interestingly, the phenyl ring of Y740 on the β9-strand is positioned in an analogous place to the purine ring of cAMP in HCN2 channels and L742 is positioned in an analogous place to the cyclic phosphate of cAMP[10]. Virtually all ion channels in the KCNH family have either tyrosine or phenylalanine at the position corresponding to Y740 in zELK and a leucine at position corresponding to L742 (Supplementary Fig. 1c). This observation raises an intriguing possibility that the β9-strand might act as an intrinsic ligand, a portion of the protein that occupies the ligand binding site whose displacement regulates the channel.

To explore a possible regulatory role of the β9-strand we examined the effect of mutations in the β9-strand on the function of intact zELK channels. zELK channels with either a point

mutation Y740A or deletion of the β9-strand (Δ740–742) exhibited robust voltage-activated currents that inactivated at voltages >+40 mV, similar to wild-type zELK channels (Supplementary Fig. 6a). However, for both mutations, the $V_{1/2}$ values for activation were significantly larger ($P<0.01$, Student's *t*-test) than the $V_{1/2}$ of wild-type channels (wild-type: −45.3±3.2 mV, n=18; Y740A: −29.8±4.4 mV, n=19; Δ740–742: −28.3±4.4 mV, n=11) (Fig. 2f and Supplementray Fig. 6b). This 15 mV shift in the voltage dependence of activation in the mutants is similar in magnitude to the effect of cAMP on HCN channels, lending further support to the possibility that the β9-strand may function as an intrinsic ligand for the zELK channels. Interestingly, mutations in the region corresponding to the β9-strand of hERG channels are associated with LQTS[20,30]. Additional experiments will need to be done to further test the intrinsic ligand hypothesis.

Similar to HCN channels, the C-linker of zELK channels is the primary region of intersubunit interactions in the crystal structure with a buried solvent accessible surface area of about 2,520 $Å^2$ for each subunit (Fig. 3a). The intersubunit interface can be likened to an "elbow-on-the-shoulder", where the "elbow" formed by the αA' and αB'-helices of one subunit is resting on the "shoulder" formed by the αD'-helix and αC'-αD' loop of the neighboring subunit (Figs. 2a, 3a,d and Supplementary Fig. 7). The structure of the "elbow-on-the-shoulder" interface between neighboring subunits is very similar between zELK and HCN2 channels (Fig. 3d), except that the region before the αD'-helix is not alpha helical in zELK.

Unexpectedly, however, the "elbow-on-the-shoulder" interface in zELK occurs with a two-fold related subunit (rotated by 180°), instead of a four-fold related subunit (rotated by 90°) like in HCN channels (Fig. 3 a,b). This difference results from a ~55° rotation in the region following the αB'-helix in zELK relative to HCN2 channels (Fig. 3c). The implication of this dramatic rotation of the "elbow" is a dimeric assembly of the C-linker/CNBHDs in the zELK structure (Fig. 3a), as opposed to the tetrameric assembly of the C-linker/CNBDs in HCN channels[10] (Fig. 3b). The intersubunit interface and the dimeric assembly are preserved in both sets of molecules in the asymmetric unit and for both crystal forms of zELK (Supplementary Fig. 8), suggesting that they are independent of crystal contacts. FSEC experiments also revealed that the GFP-tagged C-linker/CNBHD of zELK channels dimerizes at sufficiently high concentrations in solution (Supplementary Fig. 9). Additional experiments would be required to determine if the quaternary state of the C-linker/CNBHD in intact channels has a two-fold or four-fold symmetry (Supplementary Discussion and Supplementary Fig. 10).

Here we present the first crystal structure of the C-linker/CNBHD of a KCNH channel. The structure reveals a putative ligand binding pocket that differs dramatically from the cyclic nucleotide-binding pocket of HCN channels and does not appear to bind cyclic nucleotides. Instead of a ligand the putative ligand-binding pocket of zELK channels is occupied by a novel β9-strand following the αC-helix. Mutations of the β9-strand shifted the voltage dependence of activation, suggesting that the β9-strand is a regulatory element for zELK channels that acts as an intrinsic ligand. The crystal structure also displays an unexpected conformation of the C-linker that leads to dimerization of the C-linker/CNBHDs of zELK

channels. These findings provide a structural framework to understand the regulation of KCNH channels by the C-linker/CNBHD.

METHODS SUMMARY

Protein purification

The C-linker/CNBHD of zELK (amino acids Q543-L750) was subcloned into a modified pMalc2T vector (New England Biolabs) containing an N-terminal MBP affinity tag followed by a thrombin cleavage site. The protein was expressed in BL21 (DE3) *E. coli* cells as previously described[11], purified on an amylose affinity column and then on an ion-exchange column following an overnight cleavage with thrombin at 4 °C. The purified protein was concentrated to 20–30 mg/ml for crystallization. Selenomethionine derivatives were generated as previously described[10].

Crystallography

Crystals were grown at 20 °C using the sitting-drop vapor diffusion method. 150 nl drops of the concentrated protein and reservoir solutions were mixed 1:1 by a Mosquito (TTP LABTECH). The final protein solution contained: ~250 mM KCl, 1 mM TCEP, 30 mM HEPES, 100 mM citric acid, pH 3.5. The reservoir solution contained: 6% w/v 1,5-diaminopentane dihydrochloride, 180 mM ammonium acetate, 22.5% (w/v) PEG 3350, 90 mM TRIS; pH 8.5 for crystal T141; 1.8 M non-detergent sulfobetaine (NDSB)-211, 180 mM ammonium acetate, 22.5% (w/v) PEG 3350, 90 mM TRIS, pH 8.5 for crystal T42; 6% (w/v) D-(+)-galactose, 180 mM ammonium sulfate, 22.5% (w/v) PEG 3350, 90 mM HEPES, pH 7.5 for crystal T26; and 5 mM cAMP, 180 mM ammonium acetate, 22.5% (w/v) PEG 3350, 90 mM TRIS, pH 8.5 for crystal T84.

The crystallographic data are summarized in Supplementary Table 1 and details of the structure determination are described in the Online Methods.

Electrophysiology

The full length zELK channel (GI: 159570347) with a C-terminal FLAG epitope was generated by Bio Basic Inc. and subcloned into the pGEMHE oocyte expression vector. Expression of the wild-type and mutant zELK channels in *Xenopus* oocytes and current recordings were done as previously described[11]. Both pipette and bath solutions contained 130 mM KCl, 10 mM HEPES, 0.2 mM EDTA, pH 7.2. 1 mM cAMP was added to the bath solution as indicated.

METHODS

Fluorescence-detection size exclusion chromatography (FSEC)

The C-linker/CNBHD of zELK channels (amino acids Q543-L750) was covalently fused to a C-terminal GFP in the pCGFP-BC bacterial expression vector kindly provided by Kawate and Gouaux[21]. The construct was transformed into BL21 (DE3) cells. 5 ml cultures of the cells were grown at 37 °C, induced with IPTG and harvested by centrifugation. The cell pellets were resuspended in a lysis buffer (500 mM KCl, 1 mM TCEP, 30 mM HEPES,

1mM PMSF and 2.5 mg/ml DNase; pH 8.0) and sonicated. Insoluble protein was separated by centrifugation and the supernatant was analyzed on a Superdex 200 10/300 GL column (GE Healthcare).

Scale-up protein purification

The C-linker/CNBHD of zELK (amino acids Q543-L750) was subcloned into a modified pMALc2T vector (New England Biolabs) containing an N-terminal MBP affinity tag followed by a thrombin cleavage site. The protein was expressed in BL21 (DE3) *E. coli* cells as previously described[11]. The cells were harvested by centrifugation, resuspended in a lysis buffer (500 mM KCl, 1 mM TCEP, 30 mM HEPES, 1mM PMSF and 2.5 mg/ml DNase; pH 8.0) and lysed in an Emulsiflex-C5 (Avestin). Insoluble protein was separated by centrifugation. The C-linker/CNBHD of zELK was purified on an amylose affinity column and then was loaded on a HiTrap SP FF ion-exchange column following an overnight cleavage with thrombin at 4 °C. The protein was eluted with a linear KCl gradient and 100 mM citric acid (pH 3.5) was added to the final protein solution to increase the solubility of the protein at high concentrations. The protein was concentrated to 20–30 mg/ml for crystallization. Selenomethionine derivatives were generated as previously described[10,31].

Crystallization

Crystals were grown at 20 °C using the sitting-drop vapor diffusion method. 150 nl drops of the concentrated protein and reservoir solution were mixed 1:1 by a Mosquito (TTP LABTECH). The final protein solution contained: ~250 mM KCl, 1 mM TCEP, 30 mM HEPES, 100 mM citric acid, pH 3.5. The reservoir solution contained: 6% w/v 1,5-diaminopentane dihydrochloride, 180 mM ammonium acetate, 22.5% (w/v) PEG 3350, 90 mM TRIS; pH 8.5 for crystal T141; 1.8 M non-detergent sulfobetaine (NDSB)-211, 180 mM ammonium acetate, 22.5% (w/v) PEG 3350, 90 mM TRIS, pH 8.5 for crystal T42; 6% (w/v) D-(+)-galactose, 180 mM ammonium sulfate, 22.5% (w/v) PEG 3350, 90 mM HEPES, pH 7.5 for crystal T26; and 5 mM cAMP, 180 mM ammonium acetate, 22.5% (w/v) PEG 3350, 90 mM TRIS, pH 8.5 for crystal T84. The crystals were cryoprotected in reservoir solution supplemented with 25% glycerol before being flash frozen in liquid nitrogen.

Data collection and structure determination

Diffraction data sets were collected at the Advanced Light Source (beamline 8.2.1) at Lawrence Berkeley National Laboratory in Berkeley, California. Data were analyzed with Mosfilm[32] and HKL2000[33] software. Molecular replacement using the structure of the C-linker/CNBD of HCN2 channels as a search model failed to find a solution. Therefore, the structure of the zELK C-linker/CNBHD was solved by the single-wavelength anomalous dispersion (SAD) phasing of selenomethionine derivative crystal T141 using PHENIX[34] followed by numerous cycles of refinement in PHENIX and manual model building in Coot[35]. Structures for the rest of the data sets were solved by molecular replacement using the T141 structure as a search model followed by numerous cycles of refinement and manual model building. The molecular replacement was carried out using Phaser in PHENIX[34]. The asymmetric unit contained three molecules in the $C222_1$ space group and

four in the $P12_11$ space group. The structures of different zELK molecules in the asymmetric unit and molecules in the two different space groups were very similar, with RMSDs for the α carbons calculated for the entire sequence of the resolved C-linker/CNBHD ranging from 0.4 to 0.7 Å (Supplementary Fig. 8). The crystallographic data and refinement statistics are summarized in Supplementary Table 1. Electron density was visible for all but several terminal residues in molecules A and B of the native structure in the $C222_1$ space group. Molecules A and B of the native $C222_1$ structure were used for analysis in this paper. Analysis with Molprobity[36] of the final models indicated no ramachandran outliers for T141, T42 and T26 structures, and 0.59 (%) for T84. Figures were made using PyMOL[37]. The topology of the C-linker/CNBHD of zELK was defined by PROCHEK (http://www.ebi.ac.uk/pdbsum/). The phylogenetic tree in Supplementary Fig. 1a was computed with Cobalt[38] (http://www.ncbi.nlm.nih.gov/tools/cobalt/). The GI numbers for the amino acid sequences aligned in Supplementary Fig. 1c were: zELK, 159570347; hELK1, 27886667; hELK2, 26006814; hERG1, 103488986; mEAG1, 487740; bCNGA1, 231739; mHCN2, 148699724. The electrostatic potential surface calculations were carried out using the APBS[39] plugin for PyMol and the PARSE force field, and colored from red (−3 kT/e) to blue (+3 kT/e).

Electrophsyiology

The full length zELK channel (GI: 159570347) with a C-terminal FLAG epitope was generated by Bio Basic Inc. and subcloned into the pGEMHE oocyte expression vector. The cRNA was transcribed using the T7 mMessage mMachine Ultra kit (Ambion). Expression of the wild-type and mutant (Y740A and Δ 740–742) zELK channels in *Xenopus* oocytes and current recordings from inside-out patches allowing 10 min for run up following excision were done as described before[11]. Both pipette and bath solutions contained 130 mM KCl, 10 mM HEPES, 0.2 mM EDTA, pH 7.2. 1 mM cAMP was added to the bath solution as indicated. zELK currents were elicited by applying a series of 100 ms voltage pulses (ranging from −140 to +160 mV in 20 mV increments) from a prepulse potential of −140 mV, followed by a 150 ms tail pulse to −100 mV. Currents were leak-subtracted with P/4 protocol. To obtain conductance versus voltage curves, peak tail current amplitudes at −100 mV were normalized to the largest peak conductance amplitude, which followed a step to +60 mV. These normalized data were then plotted against the test voltage, and were fit with a Boltzmann equation:

$$\frac{G}{G_{max}} = \frac{1}{1+e^{\left(\frac{V-V_{1/2}}{s}\right)}} \quad (1)$$

Where V represents the test voltage, $V_{1/2}$ is the midpoint activation voltage, and s is the slope of the relation.

Supplementary Material

Refer to Web version on PubMed Central for supplementary material.

ACKNOWLEDGEMENTS

We thank M. Munari, S. Camp, S. Cunnington and G. Sheridan for excellent technical assistance. We thank the beamline staff at ALS and especially Peter Zwart for help with data analysis. We also thank the members of the Zagotta lab for helpful discussions. This work was supported by the Howard Hughes Medical Institute, the National Institutes of Health grant R01 EY010329 (W.N.Z.), and the National Institutes of Health grant F32 HL095241 (A.E.C.). The Berkeley Center for Structural Biology is supported in part by the National Institutes of Health, National Institute of General Medical Sciences, and the Howard Hughes Medical Institute. The Advanced Light Source is supported by the Director, Office of Science, Office of Basic Energy Sciences, of the U.S. Department of Energy under Contract No. DE-AC02-05CH11231.

REFERENCES

1. Sanguinetti MC, Tristani-Firouzi M. hERG potassium channels and cardiac arrhythmia. Nature. 2006; 440(7083):463–469. [PubMed: 16554806]
2. Zhang X, et al. Deletion of the potassium channel Kv12.2 causes hippocampal hyperexcitability and epilepsy. Nat Neurosci. 2010; 13(9):1056–1058. [PubMed: 20676103]
3. Camacho J. Ether a go-go potassium channels and cancer. Cancer Lett. 2006; 233(1):1–9. [PubMed: 16473665]
4. Ganetzky B, Robertson GA, Wilson GF, Trudeau MC, Titus SA. The eag family of K+ channels in Drosophila and mammals. Ann N Y Acad Sci. 1999; 868:356–369. [PubMed: 10414305]
5. Al-Owais M, Bracey K, Wray D. Role of intracellular domains in the function of the herg potassium channel. Eur Biophys J. 2009; 38(5):569–576. [PubMed: 19172259]
6. Stevens L, Ju M, Wray D. Roles of surface residues of intracellular domains of heag potassium channels. Eur Biophys J. 2009; 38(4):523–532. [PubMed: 19172261]
7. Gustina AS, Trudeau MC. hERG potassium channel gating is mediated by N- and C-terminal region interactions. J Gen Physiol. 2011; 137(3):315–325. [PubMed: 21357734]
8. Muskett FW, et al. Mechanistic insight into human ether-a-go-go-related gene (hERG) K+ channel deactivation gating from the solution structure of the EAG domain. J Biol Chem. 2011; 286(8): 6184–6191. [PubMed: 21135103]
9. Zhou Z, Gong Q, Epstein ML, January CT. HERG channel dysfunction in human long QT syndrome. Intracellular transport and functional defects. J Biol Chem. 1998; 273(33):21061–21066. [PubMed: 9694858]
10. Zagotta WN, et al. Structural basis for modulation and agonist specificity of HCN pacemaker channels. Nature. 2003; 425(6954):200–205. [PubMed: 12968185]
11. Brelidze TI, Carlson AE, Zagotta WN. Absence of direct cyclic nucleotide modulation of mEAG1 and hERG1 channels revealed with fluorescence and electrophysiological methods. J Biol Chem. 2009; 284(41):27989–27997. [PubMed: 19671703]
12. Morais Cabral JH, et al. Crystal structure and functional analysis of the HERG potassium channel N terminus: a eukaryotic PAS domain. Cell. 1998; 95(5):649–655. [PubMed: 9845367]
13. Schonherr R, Heinemann SH. Molecular determinants for activation and inactivation of HERG, a human inward rectifier potassium channel. J Physiol. 1996; 493(Pt 3):635–642. [PubMed: 8799887]
14. Wang J, Trudeau MC, Zappia AM, Robertson GA. Regulation of deactivation by an amino terminal domain in human ether-a-go-go-related gene potassium channels. J Gen Physiol. 1998; 112(5):637–647. [PubMed: 9806971]
15. Muskett FW, et al. Mechanistic insight into hERG K+ channel deactivation gating from the solution structure of the EAG domain. J Biol Chem. 2011; 286(8):6184–6191. [PubMed: 21135103]
16. Li Q, et al. NMR solution structure of the N-terminal domain of hERG and its interaction with the S4–S5 linker. Biochem Biophys Res Commun. 2010; 403(1):126–132. [PubMed: 21055387]
17. Ng CA, et al. The N-terminal tail of hERG contains an amphipathic alpha-helix that regulates channel deactivation. PLoS One. 2011; 6(1):e16191. [PubMed: 21249148]
18. Craven KB, Zagotta WN. CNG and HCN channels: two peas, one pod. Annu Rev Physiol. 2006; 68:375–401. [PubMed: 16460277]

19. Brelidze TI, Carlson AE, Davies DR, Stewart LJ, Zagotta WN. Identifying regulators for EAG1 channels with a novel electrophysiology and tryptophan fluorescence based screen. PLoS One. 2010; 5(9):e12523. [PubMed: 20824064]
20. Splawski I, et al. Spectrum of mutations in long-QT syndrome genes. KVLQT1, HERG, SCN5A, KCNE1, and KCNE2. Circulation. 2000; 102(10):1178–1185. [PubMed: 10973849]
21. Kawate T, Gouaux E. Fluorescence-detection size-exclusion chromatography for precrystallization screening of integral membrane proteins. Structure. 2006; 14(4):673–681. [PubMed: 16615909]
22. Becchetti A, et al. The functional properties of the human ether-a-go-go-like (HELK2) K+ channel. Eur J Neurosci. 2002; 16(3):415–428. [PubMed: 12193184]
23. Engeland B, Neu A, Ludwig J, Roeper J, Pongs O. Cloning and functional expression of rat ether-a-go-go-like K+ channel genes. J Physiol. 1998; 513(Pt 3):647–654. [PubMed: 9824707]
24. Trudeau MC, Titus SA, Branchaw JL, Ganetzky B, Robertson GA. Functional analysis of a mouse brain Elk-type K+ channel. J Neurosci. 1999; 19(8):2906–2918. [PubMed: 10191308]
25. Zou A, et al. Distribution and functional properties of human KCNH8 (Elk1) potassium channels. Am J Physiol Cell Physiol. 2003; 285(6):C1356–C1366. [PubMed: 12890647]
26. Rehmann H, Wittinghofer A, Bos JL. Capturing cyclic nucleotides in action: snapshots from crystallographic studies. Nat Rev Mol Cell Biol. 2007; 8(1):63–73. [PubMed: 17183361]
27. Altieri SL, et al. Structural and energetic analysis of activation by a cyclic nucleotide binding domain. J Mol Biol. 2008; 381(3):655–669. [PubMed: 18619611]
28. Clayton GM, Silverman WR, Heginbotham L, Morais-Cabral JH. Structural basis of ligand activation in a cyclic nucleotide regulated potassium channel. Cell. 2004; 119(5):615–627. [PubMed: 15550244]
29. Schunke S, Stoldt M, Lecher J, Kaupp UB, Willbold D. Structural insights into conformational changes of a cyclic nucleotide-binding domain in solution from Mesorhizobium loti K1 channel. Proc Natl Acad Sci U S A. 2011; 108(15):6121–6126. [PubMed: 21430265]
30. Napolitano C, et al. Genetic testing in the long QT syndrome: development and validation of an efficient approach to genotyping in clinical practice. JAMA. 2005; 294(23):2975–2980. [PubMed: 16414944]

METHODS REFERENCES

31. Guerrero SA, Hecht HJ, Hofmann B, Biebl H, Singh M. Production of selenomethionine-labelled proteins using simplified culture conditions and generally applicable host/vector systems. Appl Microbiol Biotechnol. 2001; 56(5–6):718–723. [PubMed: 11601620]
32. The CCP4 suite: programs for protein crystallography. Acta Crystallogr D Biol Crystallogr. 1994; 50(Pt 5):760–763. [PubMed: 15299374]
33. Otwinowski Z, Minor W. Processing X-ray diffraction data collected in oscillation mode. Methods Enzymol. 1997; 276:307–326.
34. Adams PD, et al. PHENIX: a comprehensive Python-based system for macromolecular structure solution. Acta Crystallogr D Biol Crystallogr. 2010; 66(Pt 2):213–221. [PubMed: 20124702]
35. Emsley P, Cowtan K. Coot: model-building tools for molecular graphics. Acta Crystallogr D Biol Crystallogr. 2004; 60(Pt 12 Pt 1):2126–2132. [PubMed: 15572765]
36. Chen VB, et al. MolProbity: all-atom structure validation for macromolecular crystallography. Acta Crystallogr D Biol Crystallogr. 66(Pt 1):12–21. [PubMed: 20057044]
37. DeLano, WL. The PyMOL molecular graphics system (http://www.pymol.org). DeLano Scientific, 2002
38. Hudson DH, et al. Dendroscope: an interactive viewer for large phylogenetic trees. BMC Bioinformatics. 2007; 8:460. [PubMed: 18034891]
39. Baker NA, Sept D, Joseph S, Holst MJ, McCammon JA. Electrostatics of nanosystems: application to microtubules and the ribosome. Proc Natl Acad Sci U S A. 2001; 98(18):10037–10041. [PubMed: 11517324]

40. Arnold K, Bordoli L, Kopp J, Schwede T. The SWISS-MODEL workspace: a web-based environment for protein structure homology modelling. Bioinformatics. 2006; 22(2):195–201. [PubMed: 16301204]

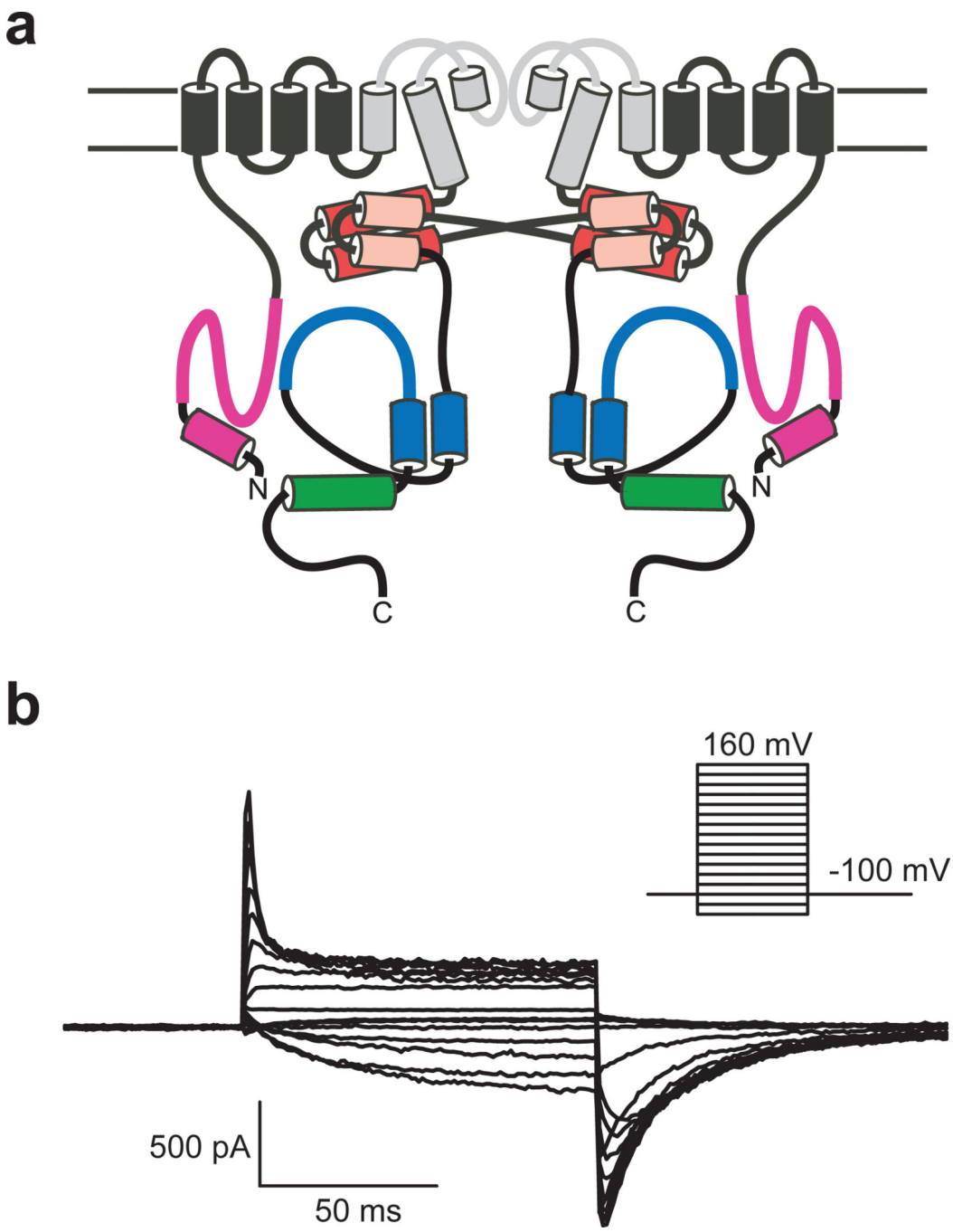

Figure 1.

Topology and electrophysiological properties of zELK channels. **a**, Cartoon of two of the four subunits of zELK channels. The pore forming loop and S5–S6 transmembrane domains are grey. The N-terminal α-helix and PAS domain are magenta. The “elbow” and “shoulder” regions of the C-linker are represented by the red and pink cylinders respectively. The αC-helix, represented by a cylinder, is green and the rest of the CNBHD is blue. **b**, Currents for zELK channels recorded in the inside-out patch configuration.

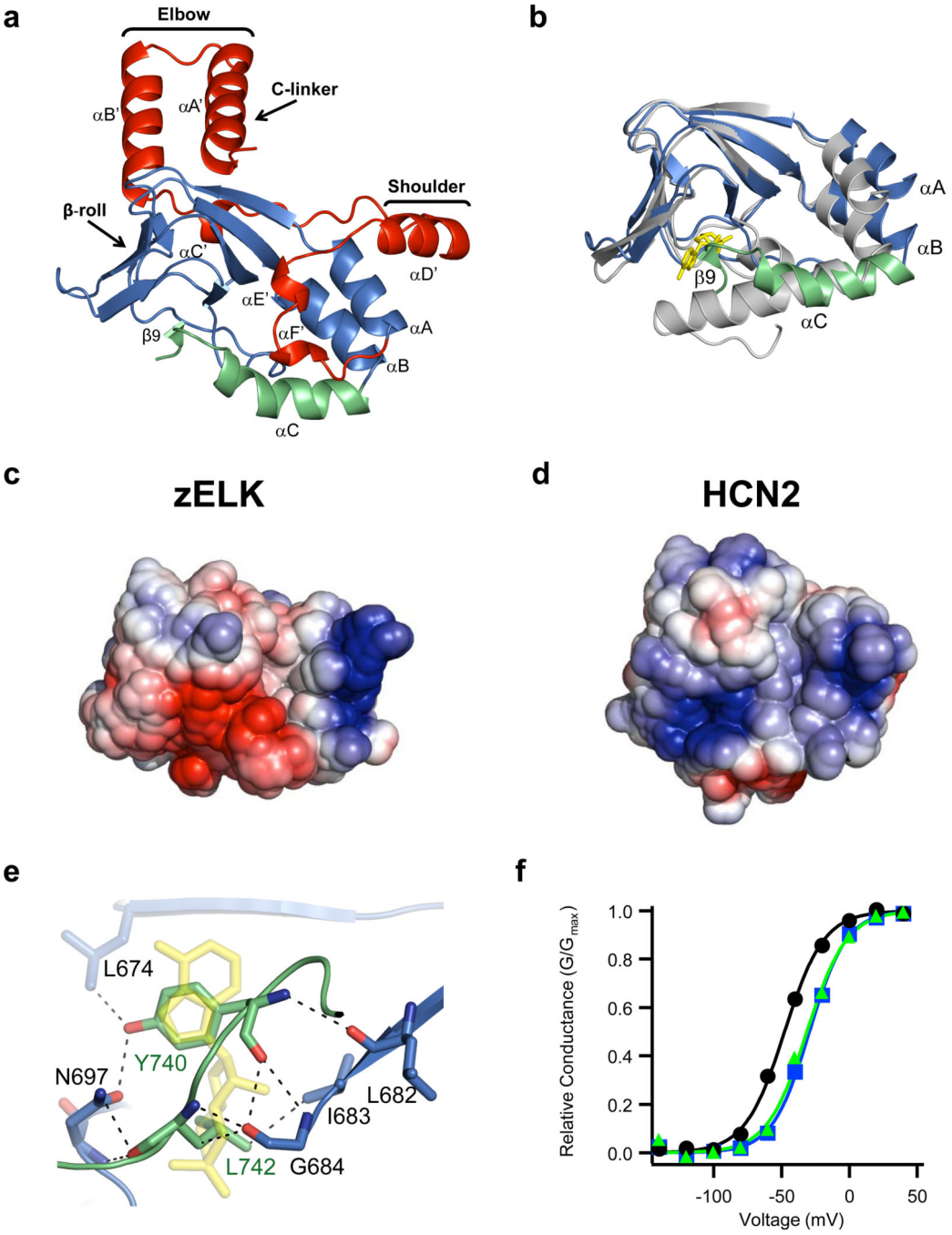

Figure 2.

Structure of the C-linker/CNBHD. **a**, Ribbon representation of a monomer of the C-linker/CNBHD of zELK channels. **b**, Alignment of the CNBHD of zELK (the αC-helix is green and the rest is blue) and HCN2 (grey) channels[10]. cAMP in the HCN2 structure is yellow. **c, d,** Electrostatic potential surface of the CNBHD of zELK (**c**) and HCN2 channels (**d**), viewed in the same orientation as in Fig. 2b. **e**, Residues in the β-roll cavity interacting with residues Y740 and L742 of the intrinsic ligand. Dashed lines show both polar and non-polar interactions. cAMP from the HCN2 structure is shown in yellow. **f**, Representative

conductance-voltage relations for wild-type (black), Y740A mutant (blue), and Δ740-742 mutant (green) zELK channels.

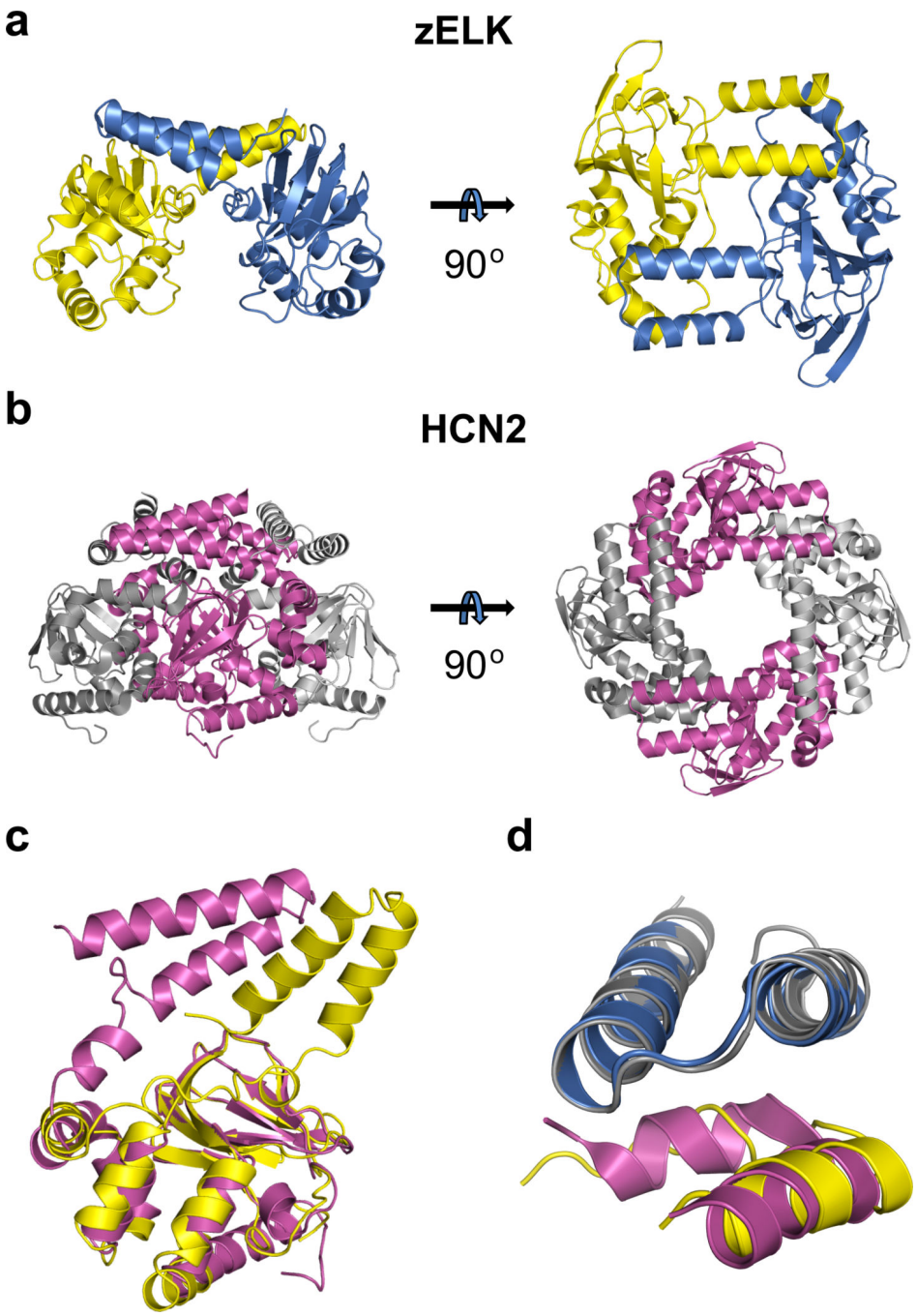

Figure 3.

Structural comparison of the C-linker regions and quaternary arrangement of the C-linker/CNBHDs of zELK and HCN2 channels. **a**, A dimer formed by the C-linker/CNBHD of zELK channels viewed perpendicular (left) and parallel (right) to the two-fold axis. **b**, A tetramer formed by the C-linker/CNBD of HCN2 channels viewed perpendicular (left) and parallel (right) to the four-fold axis. **c**, Superposition of the ribbon representations of the C-linker/CNBHDs monomers of zELK (yellow) and HCN2 channels (magenta) using the alignment of the α-carbons of CNBDs of these structures. **d**, Superposition of the "elbow-

on-the-shoulder” interface of zELK (blue “elbow”, yellow “shoulder”) and HCN2 channels (grey “elbow”, magenta “shoulder”).